Research article

Characterization and antibacterial activity of cellulose extracted from *Washingtonia robusta* and *Phoenix dactylifera* L. impregnated with eugenol: Promising wound dressing

Fatima-ezzahra Loudifa [a], Sofia Zazouli [a,*], Ikrame Nague [a], Amine Moubarik [b], Chorouk Zanane [c], Hassan Latrache [c], Ahmed Jouaiti [a]

[a] *Laboratory of Molecular Chemistry, Materials and Catalysis, Sultan Moulay Slimane University, Faculty of Sciences and Technology, B.P.523, 23000, Beni-Mellal, Morocco*
[b] *Interdisciplinary Laboratory of Research in Sciences and Technologies (LIRST), Polydisciplinary Faculty, Sultan Moulay Slimane University, BP 592, Beni-Mellal, Morocco*
[c] *Laboratory of Bio-Process and Bio-Interfaces, Faculty of Sciences and Technics, University Sultan Moulay Slimane, BP 523, 23000, Beni-Mellal, Morocco*

A B S T R A C T

This paper aimed to valorize two varieties of date palm mesh, *Washingtonia robusta* (S1) and *Phoenix Dactylifera* L. (S2) by extracting their fibrous cellulose structures for potential application in wound dressings. The extracted fibrous dressings were analyzed by using Fourier Transforms Infrareded (FTIR), X-ray diffraction (XRD), and Scanning Electron Microscopy (SEM). Additionally, mechanical properties, water absorption, and antimicrobial activity were analyzed. The results showed that S2 contained significantly higher fiber content (37.21 %) compared to S1 (12.63 %). FTIR analysis confirmed successful cellulose extraction from both palm varieties. SEM images showed that S1 fibers had a smooth-surface with smaller pores, contributing to a higher absorption capacity of 1289 $\pm$ 93 %. Therefore, S2 exhibited rougher-surfaced fibers, which enhanced its mechanical properties, as demonstrated by stress-strain tensile tests, and Young's modulus. Notably, S2 revealed superior mechanical strength compared to S1 fiber dressings. Water absorption for S2 was calculated at 509 $\pm$ 93 %. Both S1 and S2 exhibited high crystalline index (61.17 % and 62.88 %), with crystalline size of 3.54 nm for S1 and 10.03 nm for S2. Finally, Eugenol-enriched fibers showed significant activity against *E. coli* (3.8 mm and 2.3 mm), *S. aureus* (4.00 mm and 2.05 mm), and *S. epidermidis* (2.7 mm and 1.6 mm) for S1 and S2, respectively, suggesting their potential as effective new wound dressing materials.

1. Introduction

A significant fraction of human mortality is caused by secondary injuries and wound infections. On the other hand, tailored therapy and wound care assist stop pathogen invasion and minimize further damage. Wound dressings are designed to absorb exudate, maintain optimal moisture balance, prevent periwound maceration, and control bacterial growth, creating an environment conducive to healing [1]. Different forms of wound-dressing materials have been developed [2–5]. However, the perfect versatile materials to

* Corresponding author.
 *E-mail address:* sofia.zazouli@usms.ma (S. Zazouli).

simultaneously regulate blood flow and avoid bacterial infection are still lacking. Therefore, with the growth demographic ageing and the prevalence of persistent wounds and their health risk, there is an urgent need for new applicable wound care materials. Over the last decade there has been a rapid increase in interest in biopolymers and synthetic polymers, leading to several potential candidates for wound dressing applications [6–8]. Although natural polymers generally exhibit excellent biocompatibility, their application is often restricted by poor mechanical properties and limited processability [9,10]. Similarly, man-made cellulose materials, despite being renewable, face challenges in processability due to their intricate molecular structure and strong intermolecular hydrogen bonding. Consequently, they exhibit relatively low tenacity values (1.5–2.5 g/denier) compared to conventional synthetic fibers [11]. Nevertheless, these materials have proven useful in biomedical applications, particularly in the design and production of various wound dressings [12,13]. They have also been shown to accelerate wound healing by maintaining and releasing several growth factors at the damage site that encourage dermal fibroblast migration and proliferation while preventing bacterial growth in the wound [14, 15].

Cellulose, the most abundant natural polymer, is a polysaccharide made of linked glucose units [16,17]. It offers exceptional strength, flexibility, and biodegradability, making it a vital material for sustainable industrial applications [18]. With properties like high specific strength, biocompatibility, and chemical modifiability, cellulose has evolved beyond traditional uses to support emerging technologies, including nanofluid systems, where carboxymethyl cellulose (CMC) derivatives offer excellent colloidal stability and enhanced thermal conductivity [19,20]. Among the diverse sources of cellulose, palm fibers stand out as a sustainable and sustainable and cost-effective alternative [21]. As an agricultural by-product, palm cellulose is abundant, economically viable, and requires fewer resources to produce compared to bacterial cellulose, which, although superior in water retention and flexibility, involves complex and costly manufacturing processes [22]. Additionally, palm cellulose offers superior purity over wood pulp cellulose, with minimal residual lignin and hemicellulose. This makes it a more suitable choice for applications where biocompatibility and structural integrity are crucial [23]. However, the extraction of cellulose from natural fibers presents significant challenges. Methods like acid and alkaline treatments yield cellulose with varying properties, and alkalinization with sodium hydroxide (NaOH) is commonly used to improve compatibility. Yet, excessive exposure to strong alkaline solutions can degrade the cellulose structure, negatively affecting the mechanical properties of the resulting composites [24].

In recent years, there has been an increasing focus on improving the quality of wound dressings for medical applications [25]. Cellulose-based materials have proven advantageous in wound care due to their ability to maintain optimal humidity and temperature, which are essential for promoting healing. Among various sources of cellulose, algae-derived cellulose stands out due to its bioactive compounds that support natural healing and its nanostructure, which facilitates better cell interaction [26]. Similarly, bamboo-derived cellulose offers significant benefits, providing strong mechanical support and contributing to the durability and stability of wound dressings [27].

However, while these conditions support healing, they can also create a favorable environment for microbial growth [28–30]. To address this, antimicrobial agents or surface modifications are often incorporated to ensure biocompatibility and control microbial contamination [31,32]. One common approach is the inclusion of antibiotics in cellulosic textiles, which helps create antimicrobial wound dressings [33]. Another promising avenue is the use of nanotechnology, particularly metal and metal oxide nanoparticles, which exhibit strong antimicrobial activity. However, this approach carries risks, as these nanoparticles may release oxygen-free radicals that could damage human cells and potentially contribute to cancer development [34]. In response to these concerns, researchers have turned to alternative antimicrobial agents derived from herbal sources [35–37]. For instance, clove (*Syzygium aromaticum*), known for its potent antioxidant activity [38], contain eugenol (4-allyl-2-methoxyphenol, EUG) (Scheme 1) in its essential oils, which constitutes 45–90 % of the oil content Eugenol is recognized for its broad spectrum of therapeutic properties, including antimicrobial, antifungal, antioxidant, anticancer, anti-inflammatory, analgesic, repellent, and insecticidal properties [39,40]. These attributes make eugenol a promising candidate for a range of medical and industrial applications.

Despite extensive research on cellulose fibers from traditional sources like cotton and wood pulp, there is limited exploration of palm-derived cellulose fibers, particularly from *Washingtonia robusta* (S1) and *Phoenix dactylifera* L. (S2) (Fig. 1a–d), as potential biomaterials for wound dressings. The unique properties of palm fibers, such as their mechanical strength, biocompatibility, and biodegradability, remain underexplored in this context. This study aims to fill this gap by providing a comprehensive analysis of the chemical, morphological, and mechanical characteristics of these fibers, while also comparing their potential for wound healing applications with other cellulose sources. To achieve this, extractive cellulosic fibers of S1 and S2 were investigated by Fourier transform infrared-ray (FTIR), Scanning Electron Microscopy (SEM), X-ray diffraction (XRD). Additionally, the mechanical properties, including stress-strain tensile, and Young's modulus was investigated along with water absorption. Finally, the resulting fibers were
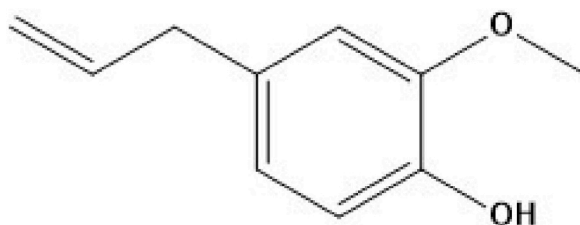
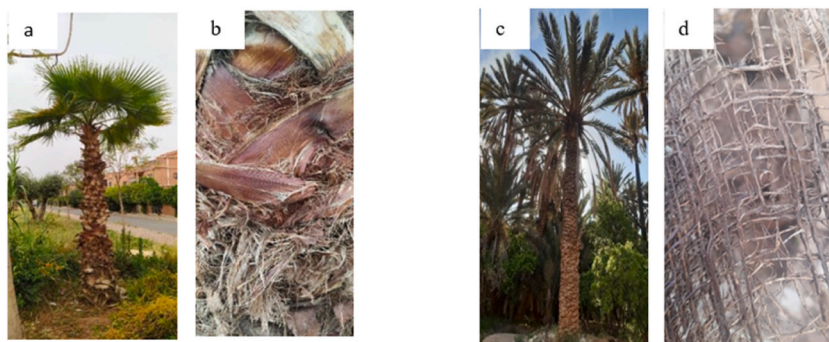**Scheme 1.** Chemical structure of 4-allyl-2-methoxyphenol.

Fig. 1. Photographs of *Washingtonia robusta* (a) *Phoenix Dactylifera* L. (c) and mesh sheets of S1 (b) and S2 (d).

enriched with eugenol, successfully extracted from clove, and their antimicrobial properties were assessed.

2. Experimental

2.1. Materials

Date palm leaf sheath (*Phoenix Dactylifera* L. (S2) and *Washingtonia robusta* (S1)) were harvested from Errachidia (31° 54′ 20.016″ N 4° 25′ 20.269″ W) and Beni Mellal (32°18′0″ N et 6°15′0″ W), respectively, during March. Cloves were also obtained from Beni Mellal. The palm samples were washed with distilled water to remove dust and other pollutants before being dried at room temperature. The collected samples (S1 and S2) were cut into 4×4cm square pieces without causing any structural damage (Fig. 3). The herbarium voucher numbers for *Phoenix dactylifera* L. and *Washingtonia robusta* are 1188 (1753) and S-PL-10056 (4276), respectively. Sigma-Aldrich provided absolute ethanol (C_2H_6O, 99 %), toluene ($C_6H_5CH_3$, 99 %), glacial acetic acid (CH_3COOH, 99.5 %), sodium hypochlorite ($NaClO_2$, 15 %), sodium hydroxide (NaOH, 98 %), sodium chloride (NaCl, 99.8 %), dichloromethane (CH_2Cl_2), magnesium sulfate anhydrous ($MgSO_4$), and hydrochloric acid (HCl).

2.2. Extraction of pure cellulose fibers

The strategy used in this study replicates several procedures employed in previous investigations [19,21,34]. *Washingtonia robusta* (S1: 0.198 g) and *Phoenix Dactylifera* L. leaf mesh samples (S2: 0.860 g) were chemically treated to isolate cellulose from hemicellulose, pectin, and lignin. Samples S1 and S2 were treated with 3 % wt NaOH solution for 3 h at 50 °C, five and eight times, respectively. The samples were then washed, dried in an oven at 40 °C and weighed (S1, yield 0.057 g; S2, yield 0.470 g). The dewaxing treatment for S1 and S2 involved using toluene-ethanol (2:1) mixture in a Soxhlet extractor for 6 h (S1, yield 0.027 g; S2, yield 0.38 g). Subsequently, the samples were treated with 15 % $NaClO_2$, 1.3 % NaOH, and a few drops of acetic acid at 60 °C for 2 h to remove natural coloring matter, revealing the creamy white color of the fibers. This treatment was repeated several times, followed by rinsing with distilled water and drying for an hour in an oven. The final yields for S1 and S2 were 0.025 g and 0.320 g, respectively.

2.3. Extraction of eugenol

The extraction of eugenol from cloves was carried out following the methods of D. Antic (2014) [43] and M. Yuwono et al. (2002) [44], with slight modifications. Fig. 2 illustrates the complete process of eugenol extraction. Initially, 10 g of ground cloves were mixed with approximately 120 mL of water in a 250 mL flask. Hydrodistillation was performed until 80 mL of distillate was collected. Then 7 g of sodium chloride was dissolved in the collected distillate, which was transferred to a separatory funnel and allowed to settle. 15 mL of dichloromethane were added to the separatory funnel, and the mixture was vigorously shaken to promote extraction. After the phases separated, magnesium sulfate was added to the organic phase to absorb any remaining water. The mixture was then filtered to remove the magnesium sulfate, leaving behind an organic phase containing a mixture of eugenol and acetyl eugenol dissolved in dichloromethane. The organic solution was then transferred to a separating funnel, and a 2 mol/L aqueous solution of sodium hydroxide was added. The funnel was shaken to ensure thorough mixing, allowing the layers to separate. The aqueous phase was collected, and the process of washing the organic phase with fresh portions of sodium hydroxide solution was repeated twice more. All collected aqueous phases were combined in a clean beaker. To complete the extraction, the pH of the combined aqueous phase was carefully adjusted to 1 using concentrated hydrochloric acid. A final liquid-liquid extraction with dichloromethane in a separating funnel to retrieve the organic phase enriched with eugenol. The solvent was then evaporated from the organic phase using a rotary evaporator (rotavap) to yield pure eugenol [44].
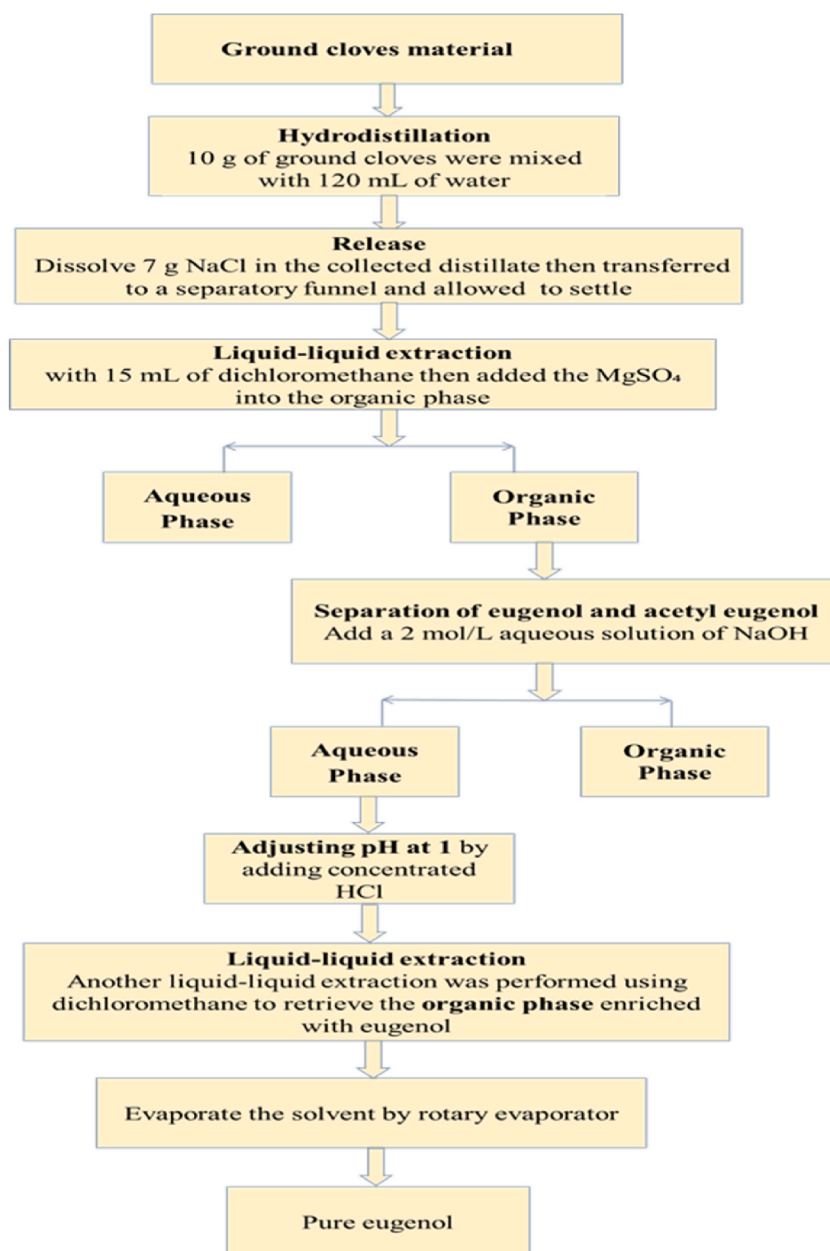
Fig. 2. The strategy for extracting eugenol from cloves.

2.4. Characterization of cellulose fibers

2.4.1. Fourier transform infrared-ray (FTIR) analysis

Fourier transform infrared-ray spectroscopy with a Tensor 27 instrument was used to analyze the functional groups of the S1 and S2 fiber dressings. Spectra were recorded in the 4000-400 cm^{-1}, using 32 scans, and were obtained in transmittance mode as a function of wave number.

2.4.2. Xray diffraction

The degrees of crystallinity of S1 and S2 fiber material was determined using X-ray diffraction (XRD) analysis. The samples were scanned with a θ-θ diffractometer, (P analytical X'Pert Pro MPD) using Cu-Kα radiation (45 KV and 40 mA). The scan angle (2θ) ranged from 3.00° to 59.99°. The crystallinity index (CrI) was calculated using the empirical Segal method [45] base on the following formula:

$$\text{CrI (\%)} = (((I_{002}) - (I_{am})) / (I_{002})) *100\% \tag{1}$$
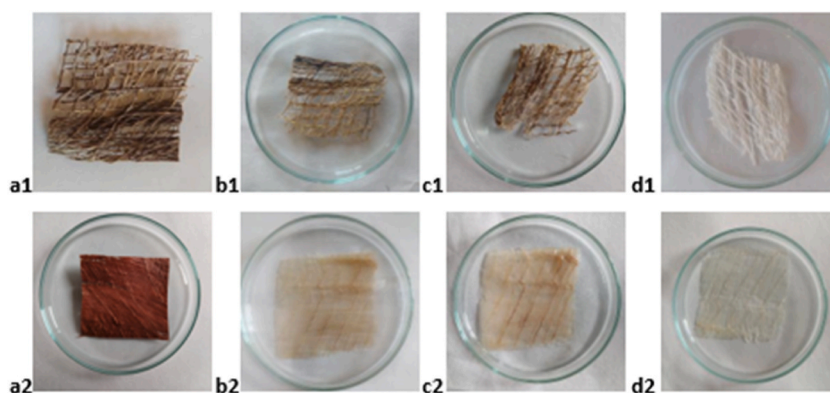
Fig. 3. Treatments required for cellulose extraction from S1 and S2. (a1, a2) raw material, (b1, b2) alkali treatment, (c1, c2) dewaxing treatment, (d1, d2) bleaching treatment.

where I_{002} is the intensity at $2\theta = 22.92°$, and I_{am} is the background scattering intensity at $2\theta = 14.96°$.

Crystallite size (CS) was calculated using the Scherrer Equation (2) [46].

$$L = \lambda.k / (\beta.cos(\theta)) \tag{2}$$

where λ is the X-ray wavelength (0.154 nm), k is the Scherrer constant (0.9), θ is the Bragg angle and β is the peak full width half maximum (FWHM).

2.4.3. SEM (scanning electron microscopy)

The surface morphology of the S1 and S2 fiber dressings was examined using a scanning electron microscope (SEM, PHILIPS XL 30 ESEM) with an accelerated voltage of 20kv. A gold-based metallizer (EMITECH K550) was used to coat the sample.

2.4.4. Mechanical properties

The mechanical properties of S1 and S2 fiber dressings were assessed by measuring tensile strain, tensile stress and Young modulus using an INSTRON 8821S testing machine (Instron, USA). Tests were conducted at a crosshead speed of 3 mm/min with a 5 kN load cell at room temperature. The relative humidity was maintained between 30 % and 40 %, in accordance with ISO 527–01, 1993 [47].

2.4.5. Water absorption measurements

The S1 and S2 samples were immersed in distilled water for 24 h at room temperature. After immersion, they were wiped with a filter paper to remove excess surface water and weighed (denoted as W0). The samples were then dried in an oven at 37 °C for 12 h and reweighed (denoted as W_1). Each sample was tested in triplicate. The water absorption coefficient (WA) of fiber dressings samples was calculated using the following formula: [48]

$$WA(\%) = ((W1 - W0) / W0)*100 \tag{3}$$

2.4.6. Antimicrobial assays

The antibacterial activity of cellulose fibers, both with and without eugenol essential oils, against *Escherichia coli* (*E. coli*; ATCC 25922), *Staphylococcus aureus* (*S. aureus*; ATCC 25923) and *Staphylococcus epidermidis* (*S. epidermis*; IPM 24728) was evaluated using an inhibition zone assay [49]. Inocula for each bacterium were prepared from a 24-h cultures grown at 37 °C in sterile Luria-Bertani liquid medium, aiming for an optical density of approximately 0.07–0.08 (approximately 10^8 UFC/mL). Antibacterial tests were conducted using young cultures in the exponential growth phase [50]. Mueller-Hinton agar was poured into sterile Petri dishes, and after solidification, 0.2 mL of the bacterial culture (concentration 10^8 UFC/mL) was evenly spread on the agar surface, with any excess liquid was removed. Cellulose fibers pieces, with and without eugenol, were then placed on these agar plates and incubated alongside the bacteria at 37 °C for 24 h. The size of the inhibition zone was determined by measuring the total diameter of the inhibition area and subtracting the diameter of the samples.

3. Results and discussion

Fig. 3a1 shows a structure characterized by a large fibrous arrangement forming a naturally woven mat of intersecting fibers of varying diameters, typical of a lignocellulosic material. In contrast the structure of S1 appears less distinct due to the presence of a layer of natural compounds arising between as shown in Fig. 3a2. After alkali treatment, the general shape of both samples remains intact, but S1begins to reveal fibers that resemble the architecture of S2, though with a thinner diameter (Fig. 3b1 and 3b2). The removal of natural wax and other impurities from the fiber surface continued through dewaxing and bleaching procedures (Fig. 3c1 and 3c2).

Visually, the untreated dry mesh fibers mats of both samples appeared dark brown, but after bleaching, they turned pale yellow or white (Fig. 3d1 and 3d2) due to the removal of lignin. The extracted cellulose content in the fiber dressings material of S2 (37.21 %) was significantly higher than for S1 (12.63 %). This higher cellulose content could contribute to better tensile properties in the fibers dressing materials. The cellulose content for S2 falls within the range of cellulose weight percentages (26.9–55.1 %) reported in several studies [51]. However, to our knowledge, the cellulose content in *Washingtonia robusta* mesh has not been previously studied.

3.1. Fourier transform infrared-ray (FTIR) analysis

The analysis was conducted on fiber dressings extracted from two distinct palm tree meshes: *Washingtonia robusta* (S1; Fig. 4a) and *Phoenix Dactylifera* L. (S2; Fig. 4b). The cellulose extracted from both samples, S1 and S2, displayed distinct absorption peak corresponding to the particular functional groups of α-cellulose in the FTIR spectra. The peaks observed in the wavenumber number range of 3660–2900 cm^{-1} characterize the stretching vibration bands of the C-H and O-H bonds in polycarbohydrates [41,42]. For each fiber dressing sample, the prominent signal at 3313 cm^{-1} corresponds to the OH group and the vibrations of inter- and intramolecular hydrogen bond in cellulose [54]. Additionally, the band at 2875 cm^{-1} (S1) and 2844 cm^{-1} (S2) are associated with the C-H stretching vibrations in polycarbohydrates [41,42]. A band at 1625 cm^{-1} was detected, corresponding to the H-O-H stretching vibration of the absorbed water. The band at 1438 cm^{-1} is assigned to C-C bond vibrations, while the band at 1313 cm^{-1} corresponds to CH_2 and CH_3 group stretches. The band at 1062 cm^{-1} is associated with the C-O group in the FT-IR spectra of the studied samples [55]. Moreover, the peak at 1031 cm^{-1} in both S1 and S2 fiber dressings is attributed to the C–O–C skeletal vibrations of the pyranose ring and β-1, 4-linked-glucopyranose unit, revealing the typical structural chemistry of cellulose [56,58]. The FTIR spectra of the cellulose-eugenol samples (S1; Fig. 4c) and (S2; Fig. 4d) reveal a robust chemical interaction, certainly involving hydrogen bonding, between the two components. New peaks observed at specific wavenumbers 1568, 1483, 1294, 1249, 912, and 834 cm^{-1} (S1), and 1570, 1486, 1300, 1240, 911, and 823 cm^{-1} (S2) along with additional shoulders at 1473 and 740 cm^{-1} in both S1 and S2, indicate conformational changes in the chemical structures of cellulose and eugenol. These peaks are linked to vibrations of C=O, C-O, and C-H bonds,
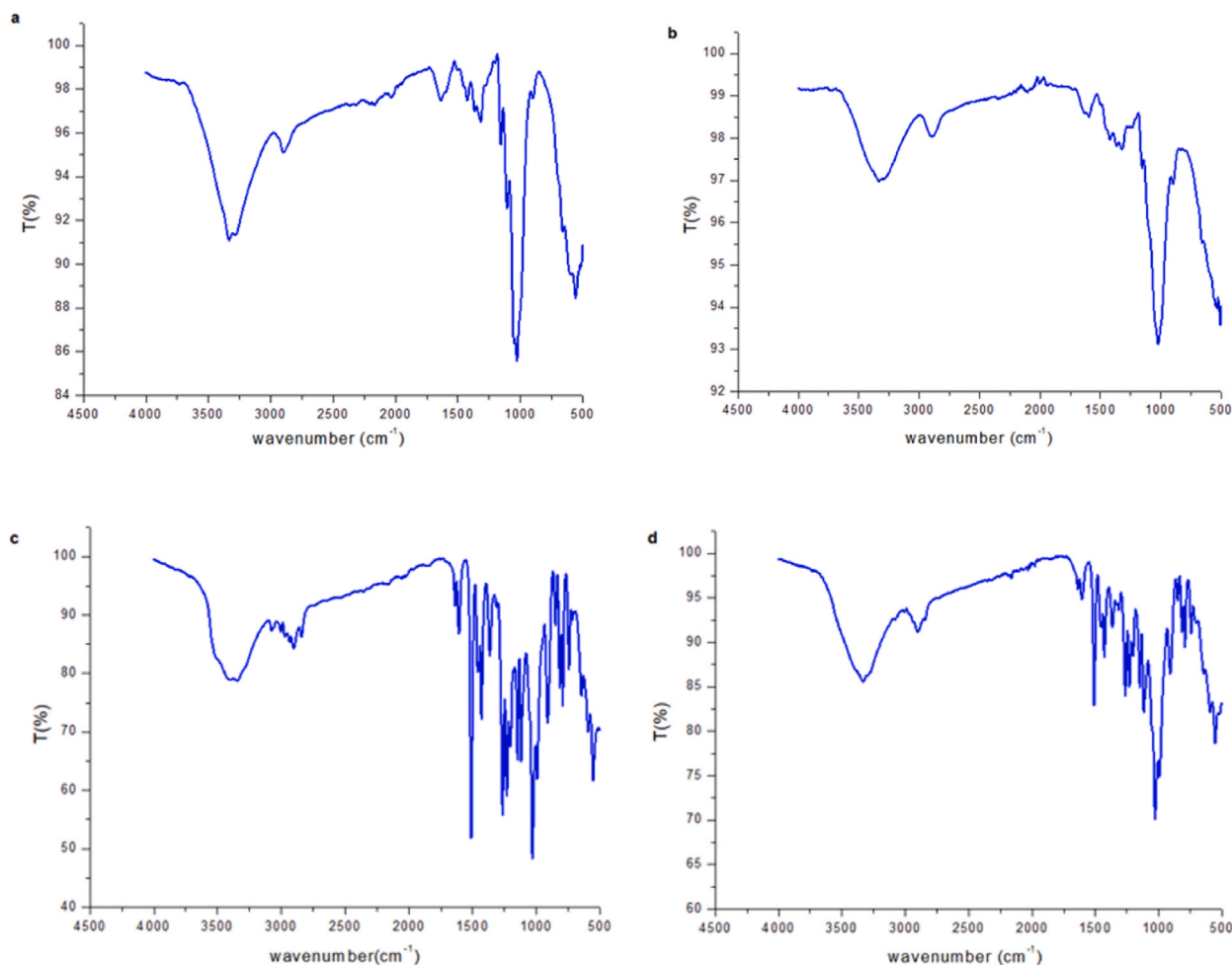

Fig. 4. FTIR spectra (a) and (b) correspond to cellulose fibers (S1) and (S2), while (c) and (d) are of cellulose-eugenol (S1) and (S2), respectively.

suggesting the formation of new chemical bonds and changes in the polymer chain [57]. Notably, peaks at lower wavelengths (<900 cm^{-1}) point to modifications in the skeletal stretching vibrations of the C-C bond. Furthermore, cellulose peaks at 1313 cm^{-1} shift to lower frequencies (1313, 1062, and 1031 cm^{-1}) in the S1 and S2 samples, suggesting a reduction in molecular order due to these conformational changes [47,48].

3.2. Xray diffraction (XRD)

Xray diffraction is a widely used method for determining the crystalline characteristics of cellulose, providing valuable insights into its mechanical and thermal properties [52]. The XRD patterns for the S1 and S2 fiber dressings are shown in Fig. 5a and b. The crystallinity index and crystallite size for both samples are presented in Table 1. The overall profiles of the S1 and S2 diffractograms are similar, both exhibiting three well-defined peaks that correspond to crystalline and amorphous region of the natural cellulose fibers. The diffraction patterns between 10° and 40° display the main peak at 14.93°, 16.73°, 22.70°, and 34.2° for S1 and at 14.96°, 16.75°, 22.72°, and 34.2° for S2. These peaks are characteristic of cellulose and correspond to the lattice planes 1−10, 110, 002, and 004, respectively. These 2θ values correspond to the regular structure of cellulose I, which impacts rigidity to the material [60]. The diffraction peaks for both crystalline phases (22.70° and 22.72°) and amorphous phases diffraction peaks (14.93°−14.96°, 16.73°−16.75°, and 34.2°) suggest that the diffractograms are characteristic of a semicrystalline material, indicating that the native cellulose fibers' structural integrity is preserved during the extraction process [53]. The crystallinity index provides information on the relative amount and structural order of crystallites within the in fibers [42]. Using Eq. (1), the crystallinity index (CI) for the isolated cellulose was calculated as 61.17 % for S1 and 62.88 % for S2 (Table 1), which is slightly comparable than that of ramie, bamboo, and flax fibers [61]. These results confirm that S2 exhibits a more organized cellulose crystalline structure than S1, which results in reduced crystallinity [50,51,62]. Additionally, Scherrer's equation (Eq. (2)) was used to calculate the crystallite sizes for S1 and S2, yielding values of 3.54 nm and 10.03 nm, respectively. This suggests indicated that S2 has a more compact crystalline structure, which likely contributes to lower moisture permeation and reduce hydrophilic behavior compared to S1 [42].

3.3. Scanning electron microscopy

Scanning electron microscopy (SEM) was used to examine the surface morphology of the fiber dressing samples, enabling an understanding of how various elements are distributed across the fiber surface [63]. The SEM analysis of S1 and S2 was carried out in the horizontal plane at different magnifications, as offered in Fig. 6. The SEM image reveal that the fibers extracted from both simples have a cylindrical shape with distinct morphological surfaces. A study by Filho et al. (2023) highlighted the unique fiber structures of cellulosic materials, including the web-like clustering of cellulose fibers, which aligns with the observations made in this study [64]. Specifically, the fiber dressing of S1 exhibits a compact and continuous structure moderately smooth surface, likely due to the presence of a waxy coating on its exterior as noted in previous research [65]. Additionally, S1 displays several small, unevenly spaced pits with an almost round oval shape, ranging in diameter from 4.68 to 15.62 μm. These pits are important for wood healing, as they facilitate gas and nutrient diffusion, cell migration and tissue development [66]. In contrast, the SEM of S2 shows a rough and flaky surface with some ruptured and less regular fibers alignment, which may results from defibrillation and the removal of some surface constituents such as wax and other layers [67]. The increasing roughness on the outer layer is a key feature that facilitates cell attachment, which is important for healing dressings. Moreover, the diameter of the cellulose fiber in S2 (522.22 μm) is comparatively larger than that in S1, which is estimated to be 251.11 μm.
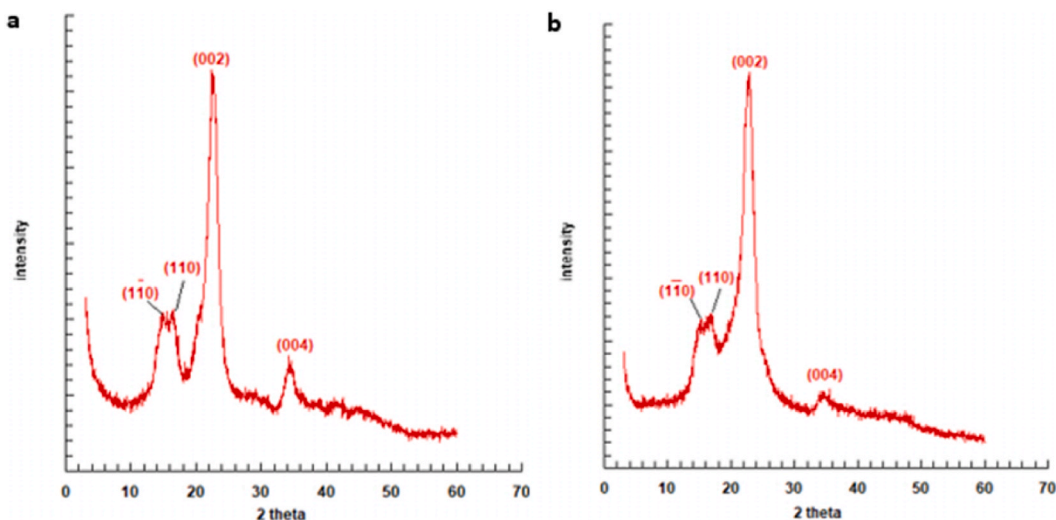

Fig. 5. XRD diffractogram of (a) S1 and (b) S2.

Table 1
Crystallinity index, crystallite size, mechanical properties and water absorption of studies samples.

Samples	Crystallinity Index (%)	Crystallite Size (nm)	Mechanical properties			Water absorption (%)
			Young's modulus (GPa)	Tensile Strength (%)	Tensile Stress (Mpa)	
S1	61.17	3.54	13.7 ± 1.53	1.4 ± 0.15	463 ± 40	1289 ± 93
S2	62.88	10.03	22.3 ± 3.51	1.2 ± 0.15	618 ± 34	509 ± 66
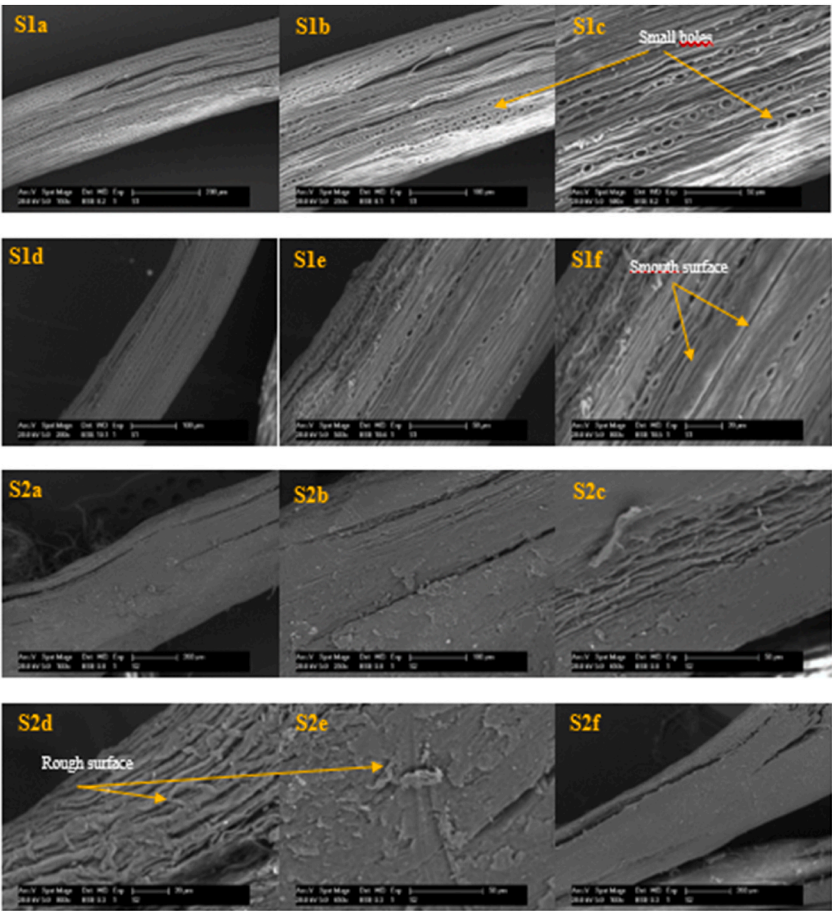
Fig. 6. SEM micrographs of cellulose fibers of S1 and S2.

3.4. Mechanical properties

Mechanical strength is a critical factor when assessing materials for use as wound dressings. A wound dressing must be strong, flexible, and resistant to rupture during use, whether applied topically to cover a skin wound or used internally for wound protection [70,71]. The mechanical properties of S1 and S2 are evaluated based on Young's modulus and the stress-strain data recorded during tensile testing. The results are summarized in Table 1. Both fiber dressings, S1 and S2 demonstrated high tensile strengths of 463 ± 40 MPa and 618 ± 34 MPa, respectively, with Young's modulus of 13.7 ± 1.53 GPa for S1 and 22.3 ± 3.51 GPa for S2, indicating excellent mechanical tensile properties, especially for S2. These findings are consistent with previous research by Munawar et al. (2007), who reported high tensile strength characteristics in natural fibers such as ramie bast fiber, sisal, and pineapple fiber [68]. The observed differences in mechanical performance can be attributed to the porous structure and the reduced crystallinity of S1, as evidenced by the Scanning Electron Microscopy and X-ray diffraction analyses conducted in this study. In addition, S1 and S2 fiber dressings presented tensile strains of 1.4 ± 0.15 % and 1.2 ± 0.15 %, respectively, which are lower than those of previously reported wound dressings [38, 40,56]. Despite this, the samples still show potential for use as wound dressing, with the possibility of improving their mechanical properties further for enhanced performance.

3.5. Water absorption measurements

Water absorption is a critical characteristic of wound dressings. Moist and wet dressings help stimulate re-epithelialization, accelerate wound healing, and minimize scarring while ensuring that the dressings can be removing without damaging fresh tissue [72]. The water absorption was determined using Eq. (3), and the results are presented in Table 1. Fiber dressings made from date palm mesh. Both samples S1 and S2 samples demonstrated good water absorption capabilities, revealing that they can maintain a moist environment conductive to wound healing. However, the water absorption of the S1 fiber dressing (1289 ± 93 %) was significantly higher than that of the S2 fiber dressing (509 ± 66 %). This difference may be attributed to the presence of micron-sized holes on the outer-layer of the S1 fiber dressing, which likely enhances water absorption retention by allowing larger volumes of water to be absorbed. These results are in line with those reported by Begum et al. (2021) for cotton, where similar absorption characteristics were observed [73]. Furthermore, the higher water absorption in S1 is consistent with the observations made in the Xray diffraction analysis.

3.6. Antimicrobial activity

Chronic bacterial infections are a major factor in delayed wound healing, underscoring the critical demand for antimicrobial fiber materials [69]. In this study, we evaluated the antibacterial properties of cellulose fibers enriched with eugenol against *E. coli*, *S. aureus*, and *S. epidermidis*. The assessment was conducted in vitro by measuring the inhibition zones of each sample, with the results depicted in Fig. 7. Cellulose fibers without eugenol from both samples S1 and S2 exhibited no inhibitory effect against the three bacterial strains. This lack of inhibition can be attributed to the biopolymer's fully organic chemical structure, which make it highly
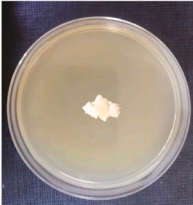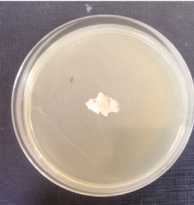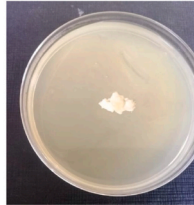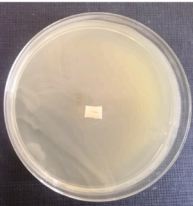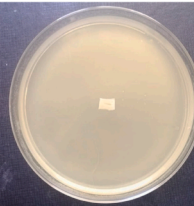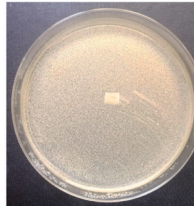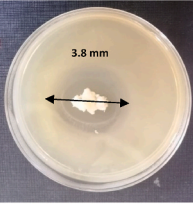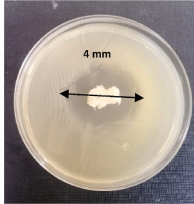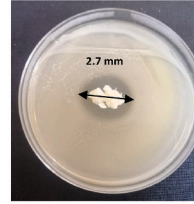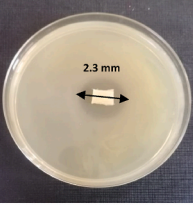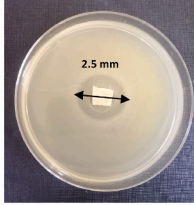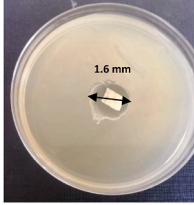

Fig. 7. Visualization of inhibition zones for cellulose, cellulose-eugenol against *Escherichia coli*, *Staphylococcus aureus*, and *Staphylococcus epidermidis*.

susceptible to microbial attack [74]. However, the addition of eugenol significantly increased the inhibition zones for all tested bacterial strains in both S1 and S2. The size of the inhibition zone generally reflects the antimicrobial activity of the samples, with a larger zone, indicating greater effectiveness of the antimicrobial effectiveness. Comparing the samples, it is evident that the inhibition zone for S1 (3.8 mm, 4.00 mm, 2.7 mm) was larger than for S2 (2.3 mm, 2.5 mm, 1.6 mm) (Table 2). This difference indicates that S1 has absorbed a significant amount of eugenol due to its porous surface, as observed in the SEM analysis. Additionally, eugenol essential oil exhibited well-defined zones of inhibition, further demonstrating its effective biocidal properties [59,75]. Notably, no significant differences in antimicrobial activity were observed between Gram-positive and Gram-negative bacteria. Eugenol, a bioactive compound, has been shown to exhibit significant antimicrobial activity by disrupting the lipid bilayer of bacterial membranes, as demonstrated by G. Ebenezer Jeyakumar et al. (2021) [76]. This disruption increases membrane permeability, leading to the leakage of intracellular components, such as ATP and essential nutrients, ultimately leading to cell death. By destabilizing the bacterial membrane, eugenol effectively inhibits the growth of both pathogens, making it a promising antibacterial agent.

4. Conclusion

Cellulosic Fiber dressings were successfully extracted from *Washingtonia robusta* and *Phoenix Dactylifera* L. tree mesh, which is abundant in Morocco. We analyzed their chemical, molecular structure groups, morphological, water absorption, mechanical properties, and antibacterial activity. FTIR analysis revealed functional groups similar to those found in other cellulosic fibers, with significant loss of hemicellulose and lignin during alkali treatment and bleaching, resulting in 37.21 % cellulose content for S2, which was higher than S1 (12.63 %). X-ray diffraction confirmed the presence of native cellulose, with crystalline sizes of 3.54 nm (S1) and 10.03 nm (S2) and crystallinity index of 61.17 % and 62.88 %, respectively. SEM imaging showed a smooth, porous surface for S1 and a rougher surface for S2, due to the removal of lignin and hemicellulose. The mechanical analysis demonstrated that S2's higher cellulose content and crystallinity improved its tensile properties. Furthermore, S1 exhibited higher water absorption (1289 ± 93 %) compared to S2, (509 ± 66 %), which ensures a moist environment ideal for dressing wounds. Eugenol, extracted from cloves, was successfully incorporated into the fibers, significantly enhancing their antibacterial activity. The cellulose-eugenol composites displayed strong inhibition against *E. coli* (3.8 mm and 2.3 mm), *S. aureus* (4.00 mm and 2.05 mm), and *S. epidermidis* (2.7 mm and 1.6 mm) for S1 and S2, respectively. This combination of cellulose and eugenol provides both structural support and antimicrobial properties, making these fiber dressings highly promising for wound care applications. Future research will focus on clinical trials to further evaluate their effectiveness.

CRediT authorship contribution statement

Fatima-ezzahra Loudifa: Writing – original draft, Formal analysis. **Sofia Zazouli:** Writing – review & editing, Methodology, Investigation. **Ikrame Nague:** Writing – review & editing, Investigation, Formal analysis. **Amine Moubarik:** Resources. **Chorouk Zanane:** Resources. **Hassan Latrache:** Resources. **Ahmed Jouaiti:** Resources, Project administration, Methodology, Conceptualization.

Data availability statement

Data included in the article is referenced in the article.

Ethics statement

This research fully complies with the ethical standards outlined by *HELIYON*. After a thorough review of the ethics declarations available at [https://www.cell.com/heliyon/ethics], we have ensured that all relevant statements are incorporated into the ethical considerations section of this manuscript.

The authors affirm that there are no conflicts of interest related to this research. The study was conducted with full impartiality, free from any external influences that could potentially affect the integrity of the results. Data collection and analysis adhered to stringent methodological standards, ensuring both accuracy and transparency throughout the process.

The authorship of this manuscript accurately reflects the contributions of each individual author. All authors have reviewed and given their approval for the final version of the manuscript prior to submission. This manuscript represents original work, with appropriate acknowledgment to our institution, the University Sultan Moulay Slimane. No part of this manuscript has been plagiarized. Additionally, this study does not involve human or animal subjects, and there are no ethical concerns regarding human or animal welfare associated with the research.

Funding statement

This research did not receive any specific funding or grants from public, commercial, or not-for-profit funding agencies.

Declaration of competing interest

The authors declare that they have no known competing financial interests or personal relationships that could have appeared to

Table 2

Inhibition Zones for cellulose, cellulose-eugenol against *Escherichia coli*, *Staphylococcus aureus*, and *Staphylococcus epidermidis*.

Samples	Inhibition zones (mm)		
	Escherichia coli	*Staphylococcus aureus*	*Staphylococcus epidermidis*
S1	0.00	0.00	0.00
S2	0.00	0.00	0.00
S1- eugenol	3.8	4.00	2.7
S2- eugenol	2.3	2.5	1.6

influence the work reported in this paper.

References

[1] J. Osorio Echavarría, N.A. Gómez Vanegas, C.P.O. Orozco, Chitosan/carboxymethyl cellulose wound dressings supplemented with biologically synthesized silver nanoparticles from the ligninolytic fungus Anamorphous Bjerkandera sp. R1, Heliyon (2022) e10258, https://doi.org/10.1016/j.heliyon.2022.e10258.

[2] M. Guo, P. Kim, G. Li, C.G. Elowsky, J.R. Alfano, "A bacterial effector Co-opts calmodulin to target the plant microtubule network, Cell Host Microbe (2016) 67–78, https://doi.org/10.1016/j.chom.2015.12.007.

[3] X. Yang, et al., Pharmaceutical intermediate-modified gold nanoparticles: against multidrug-resistant bacteria and wound-healing application via an electrospun scaffold, ACS Nano (2017) 5737–5745, https://doi.org/10.1021/acsnano.7b01240.

[4] L. Shang, Y. Cheng, Y. Zhao, Emerging droplet microfluidics, Chem. Rev. (2017) 7964–8040, https://doi.org/10.1021/acs.chemrev.6b00848.

[5] A. Memic, T. Abudula, H.S. Mohammed, K. Joshi Navare, T. Colombani, S.A. Bencherif, Latest progress in electrospun nanofibers for wound healing applications, ACS Appl. Bio Mater. (2019) 952–969, https://doi.org/10.1021/acsabm.8b00637.

[6] F. Karadeniz, H.K. Sung, H.S. Kim, Natural origin polymers: applications as wound care materials, J. Life Sci. (2019) 382–393, https://doi.org/10.5352/JLS.2019.29.3.382.

[7] B.A. Aderibigbe, B. Buyana, Alginate in wound dressings, Pharmaceutics (2018), https://doi.org/10.3390/pharmaceutics10020042.

[8] V. Vivcharenko, A. Przekora, Modifications of wound dressings with bioactive agents to achieve improved pro-healing properties, Appl. Sci. (2021), https://doi.org/10.3390/app11094114.

[9] Z. Obagi, G. Damiani, A. Grada, V. Falanga, Principles of wound dressings: a review, Surg. Technol. Int. (2019) 1–8.

[10] Y. Zhong, H. Xiao, F. Seidi, Y. Jin, Natural polymer-based antimicrobial hydrogels without synthetic antibiotics as wound dressings, Biomacromolecules (2020) 2983–3006, https://doi.org/10.1021/acs.biomac.0c00760.

[11] S. Devi, et al., Characterization of natural fiber extracted from corn (Zea mays L.) stalk waste for sustainable development, Sustain. (2022), https://doi.org/10.3390/su142416605.

[12] M. Alsahag, et al., Preparation of carboxymethyl cellulose/polyvinyl alcohol wound dressing composite immobilized with anthocyanin extract for colorimetric monitoring of wound healing and prevention of wound infection, Int. J. Biol. Macromol. (2023) 233–242, https://doi.org/10.1016/j.ijbiomac.2022.10.119.

[13] H.P.S. Abdul Khalil, et al., A review on plant cellulose nanofibre-based aerogels for biomedical applications, Polymers (2020), https://doi.org/10.3390/polym12081759.

[14] B.M. Cullen, D.W. Silcock, C. Boyle, Wound Dressing Comprising Oxidized Cellulose and Human Recombinant Collagen, U.S. Pat, 2010.

[15] S. Alven, B.A. Aderibigbe, Chitosan and cellulose-based hydrogels for wound management, Int. J. Mol. Sci. (2020) 1–30, https://doi.org/10.3390/ijms21249656.

[16] S. Rbihi, L. Laallam, M. Sajieddine, A. Jouaiti, Characterization and thermal conductivity of cellulose based composite xerogels, Heliyon (2019) e01704, https://doi.org/10.1016/j.heliyon.2019.e01704.

[17] H. Atmani, S. Zazouli, F. Ezzahra Bakkardouch, L. Laallam, A. Jouaiti, Insights into interactions of cellulose acetate and metal ions (Zn2+, Cu2+, and Ag+) in aqueous media using DFT study, Comput. Theor. Chem. (2021), https://doi.org/10.1016/j.comptc.2021.113322.

[18] B.T. Wang, S. Hu, X.Y. Yu, L. Jin, Y.J. Zhu, F.J. Jin, Studies of cellulose and starch utilization and the regulatory mechanisms of related enzymes in Fungi, Polymers (2020) 1–17, https://doi.org/10.3390/polym12030530.

[19] D. Rahmadiawan, et al., Experimental investigation on stability, tribological, viscosity, and thermal conductivity of MXene/Carboxymethyl cellulose (CMC) water-based nanofluid lubricant, J. Tribol. (2023) 36–50.

[20] S.C. Shi, S.W. Ouyang, D. Rahmadiawan, Erythrosine–dialdehyde cellulose nanocrystal coatings for antibacterial paper packaging, Polymers (2024) 1–11, https://doi.org/10.3390/polym16070960.

[21] H.N. Dhakal, S.H. Khan, I.A. Alnaser, M.R. Karim, A. Saifullah, Z. Zhang, Potential of date palm fibers (DPFs) as a sustainable reinforcement for bio- composites and its property enhancement for key applications: a review, Macro Mol. Mater. Eng. (2024), https://doi.org/10.1002/mame.202400081.

[22] R. Portela, C.R. Leal, P.L. Almeida, R.G. Sobral, Bacterial cellulose: a versatile biopolymer for wound dressing applications, Microb. Biotechnol. (2019) 586–610, https://doi.org/10.1111/1751-7915.13392.

[23] A. Ferrer, I. Filpponen, A. Rodríguez, J. Laine, O.J. Rojas, Valorization of residual empty palm fruit bunch fibers (EPFBF) by microfluidization: production of nanofibrillated cellulose and EPFBF nanopaper, Bioresour. Technol. (2012) 249–255, https://doi.org/10.1016/j.biortech.2012.08.108.

[24] H. Abral, et al., Alkali treatment of screw pine (Pandanus odoratissimus) fibers and its effect on unsaturated polyester composites, Polym. Plast. Technol. Eng. (2012) 12–18, https://doi.org/10.1080/03602559.2011.593090.

[25] C.K. Bower, et al., Protein antimicrobial barriers to bacterial adhesion: in vitro and in vivo evaluation of nisin-treated implantable materials, Colloids Surf. B Biointerfaces (2002) 81–90, https://doi.org/10.1016/S0927-7765(01)00318-6.

[26] B. Machado, S.M. Costa, I. Costa, R. Fangueiro, D.P. Ferreira, The potential of algae as a source of cellulose and its derivatives for biomedical applications, Cellulose (2024) 3353–3376, https://doi.org/10.1007/s10570-024-05816-w.

[27] X. Cao, et al., Cellulose-based functional hydrogels derived from bamboo for product design, Front. Plant Sci. (2022) 1–12, https://doi.org/10.3389/fpls.2022.958066.

[28] Y. Qiu, et al., The effects of ventilation, humidity, and temperature on bacterial growth and bacterial genera distribution, Int. J. Environ. Res. Publ. Health (2022), https://doi.org/10.3390/ijerph192215345.

[29] R. Dastjerdi, M.R.M. Mojtahedi, A.M. Shoshtari, A. Khosroshahi, Investigating the production and properties of Ag/TiO2/PP antibacterial nanocomposite filament yarns, J. Text. Inst. (2010) 204–213, https://doi.org/10.1080/00405000802346388.

[30] S. S, Developments in wound dressings, Curr. Trends Fash. Technol. Text. Eng. (2018) 8–10, https://doi.org/10.19080/ctftte.2018.02.555578.

[31] S. Parham, et al., Textile/Al2O3-TiO2 nanocomposite as an antimicrobial and radical scavenger wound dressing, RSC Adv. (2016) 8188–8197, https://doi.org/10.1039/c5ra20361a.

[32] S. Parham, D.H.B. Wicaksono, S. Bagherbaigi, S.L. Lee, H. Nur, Antimicrobial treatment of different metal oxide nanoparticles: a critical review, J. Chinese Chem. Soc. (2016) 385–393, https://doi.org/10.1002/jccs.201500446.

[33] S. Parham, M. Nemati, S. Sadir, S. Bagherbaigi, D.H.B. Wicaksono, H. Nur, In situ synthesis of silver nanoparticles for Ag-NP/Cotton nanocomposite and its bactericidal effect, J. Chinese Chem. Soc. (2017) 1286–1293, https://doi.org/10.1002/jccs.201700157.

[34] S. Parham, D.H.B. Wicaksono, H. Nur, A proposed mechanism of action of textile/Al2O3–TiO2 bimetal oxide nanocomposite as an antimicrobial agent, J. Text. Inst. (2019) 791–798, https://doi.org/10.1080/00405000.2018.1526445.

[35] K. Wińska, W. Mączka, J. Łyczko, M. Grabarczyk, A. Czubaszek, A. Szumny, Essential oils as antimicrobial agents—myth or real alternative? Molecules (2019) 1–21, https://doi.org/10.3390/molecules24112130.

[36] P. Knezevic, V. Aleksic, N. Simin, E. Svircev, A. Petrovic, N. Mimica-Dukic, Antimicrobial activity of Eucalyptus camaldulensis essential oils and their interactions with conventional antimicrobial agents against multi-drug resistant Acinetobacter baumannii, J. Ethnopharmacol. (2016) 125–136, https://doi.org/10.1016/j.jep.2015.12.008.

[37] R.G. Saratale, G. Benelli, G. Kumar, D.S. Kim, G.D. Saratale, Bio-fabrication of silver nanoparticles using the leaf extract of an ancient herbal medicine, dandelion (Taraxacum officinale), evaluation of their antioxidant, anticancer potential, and antimicrobial activity against phytopathogens, Environ. Sci. Pollut. Res. (2018) 10392–10406, https://doi.org/10.1007/s11356-017-9581-5.

[38] D.C. Sinica, Syzygium aromaticum (clove), PlantwisePlus Knowl. Bank Species Pa (2022) 120–125, https://doi.org/10.1079/pwkb.species.52412.

[39] A. Kowalewska, K. Majewska-smolarek, Eugenol-Based Polymeric Materials — Antibacterial Activity doses for long periods of time. Therefore, a growing interest in eu Keywords: essential oils of cinnamon, bay and tulsi leaves, turmeric, nutm Syzygium aromaticum activities of this compound, 2023.

[40] F.J.B. Gomes, J.L. Colodette, A. Burnet, L.A.R. Batalha, F.A. Santos, I.F. Demuner, Thorough characterization of Brazilian new generation of eucalypt clones and grass for pulp production, Int. J. For. Res. (2015) 1–10, https://doi.org/10.1155/2015/814071.

[41] M.P. Grimaldi, M.P. Marques, C. Laluce, E.M. Cilli, S.R.P. Sponchiado, Evaluation of lime and hydrothermal pretreatments for efficient enzymatic hydrolysis of raw sugarcane bagasse, Biotechnol. Biofuels (2015) 1–14, https://doi.org/10.1186/s13068-015-0384-y.

[42] N. Johar, I. Ahmad, A. Dufresne, Extraction, preparation and characterization of cellulose fibres and nanocrystals from rice husk, Ind. Crops Prod. (2012) 93–99, https://doi.org/10.1016/j.indcrop.2011.12.016.

[43] D. Antic, picoSpin TM 45/80 : Extraction of Eugenol from Cloves, 2014.

[44] M. Yuwono, A.F. Hafid, A.T. Poemorno, M. Agil, G. Indrayanto, EUGENOL, 2002, pp. 149–177.

[45] L. Segal, J.J. Creely, A.E. Martin, C.M. Conrad, An empirical method for estimating the degree of crystallinity of native cellulose using the X-ray diffractometer, Textil. Res. J. (1959) 786–794, https://doi.org/10.1177/004051755902901003.

[46] S.S. Saravanakumar, A. Kumaravel, T. Nagarajan, P. Sudhakar, R. Baskaran, Characterization of a novel natural cellulosic fiber from Prosopis juliflora bark, Carbohydr. Polym. (2013) 1928–1933, https://doi.org/10.1016/j.carbpol.2012.11.064.

[47] ISO, ISO 527-1:2019, Plastics—Determination of Tensile Properties—Part 1: General Principles, 2006.

[48] R.T.A. Machado, et al., Komagataeibacter rhaeticus grown in sugarcane molasses-supplemented culture medium as a strategy for enhancing bacterial cellulose production, Ind. Crops Prod. (2018) 637–646, https://doi.org/10.1016/j.indcrop.2018.06.048.

[49] P. Ngamsurach, P. Praipipat, Antibacterial activities against Staphylococcus aureus and Escherichia coli of extracted Piper betle leaf materials by disc diffusion assay and batch experiments, RSC Adv. (2022) 26435–26454, https://doi.org/10.1039/d2ra04611c.

[50] S. Akhramez, et al., Synthesis of pyrazolo-enaminones, bipyrazoles and pyrazolopyrimidines and evaluation of antioxidant and antimicrobial properties, Arab. J. Chem. (2022), https://doi.org/10.1016/j.arabjc.2021.103527.

[51] S. Awad, Y. Zhou, E. Katsou, Y. Li, M. Fan, A critical review on date palm tree (Phoenix dactylifera L.) fibres and their uses, in: Bio-composites, Springer Netherlands, 2021, https://doi.org/10.1007/s12649-020-01105-2.

[52] M.F. Rosa, et al., Cellulose nanowhiskers from coconut husk fibers: effect of preparation conditions on their thermal and morphological behavior, Carbohydr. Polym. (2010) 83–92, https://doi.org/10.1016/j.carbpol.2010.01.059.

[53] M. Poletto, V. Pistor, M. Zeni, A.J. Zattera, Crystalline properties and decomposition kinetics of cellulose fibers in wood pulp obtained by two pulping processes, Polym. Degrad. Stabil. (2011) 679–685, https://doi.org/10.1016/j.polymdegradstab.2010.12.007.

[54] M.C. Popescu, C.M. Popescu, G. Lisa, Y. Sakata, Evaluation of morphological and chemical aspects of different wood species by spectroscopy and thermal methods, J. Mol. Struct. (2011) 65–72, https://doi.org/10.1016/j.molstruc.2010.12.004.

[55] N.A.N. Mohamad, J. Jai, Response surface methodology for optimization of cellulose extraction from banana stem using NaOH-EDTA for pulp and papermaking, Heliyon (2022) e09114, https://doi.org/10.1016/j.heliyon.2022.e09114.

[56] D. Das, S. Hussain, A.K. Ghosh, A.K. Pal, Studies on cellulose nanocrystals extracted from Musa sapientum: structural and bonding aspects, Cellul. Chem. Technol. (2018) 729–739.

[57] Y. Qin, W. Li, D. Liu, M. Yuan, L. Li, Development of active packaging film made from poly (lactic acid) incorporated essential oil, Prog. Org. Coating (2017) 76–82, https://doi.org/10.1016/j.porgcoat.2016.10.017.

[58] S. Fakhreddin Hosseini, M. Rezaei, M. Zandi, F.F. Ghavi, Preparation and functional properties of fish gelatin-chitosan blend edible films, Food Chem. (2013) 1490–1495, https://doi.org/10.1016/j.foodchem.2012.09.081.

[59] M. Ahmad, S. Benjakul, T. Prodpran, T.W. Agustini, Physico-mechanical and antimicrobial properties of gelatin film from the skin of unicorn leatherjacket incorporated with essential oils, Food Hydrocolloids (2012) 189–199, https://doi.org/10.1016/j.foodhyd.2011.12.003.

[60] L.R. Schroeder, V.M. Gentile, R.H. Atalla, Nondegradative preparation of amorphous cellulose, J. Wood Chem. Technol. (1986) 1–14, https://doi.org/10.1080/02773818608085213.

[61] T. Zhang, M. Guo, L. Cheng, X. Li, Investigations on the structure and properties of palm leaf sheath fiber, Cellulose (2015) 1039–1051, https://doi.org/10.1007/s10570-015-0570-x.

[62] M.D. Alotaibi, et al., Characterization of natural fiber obtained from different parts of date palm tree (Phoenix dactylifera L.), Int. J. Biol. Macromol. (2019) 69–76, https://doi.org/10.1016/j.ijbiomac.2019.05.102.

[63] L.A. Elseify, M. Midani, A.H. Hassanin, T. Hamouda, R. Khiari, Long textile fibres from the midrib of date palm: physiochemical, morphological, and mechanical properties, Ind. Crops Prod. (2020), https://doi.org/10.1016/j.indcrop.2020.112466.

[64] A. Valério Filho, et al., Extraction of fatty acids and cellulose from the biomass of algae Durvillaea antarctica and Ulva lactuca: an alternative for biorefineries, Algal Res. (March 2023), https://doi.org/10.1016/j.algal.2023.103084.

[65] J. De, R.N. Baxi, Experimental investigation and analysis of mercerized and citric acid surface treated bamboo fiber reinforced composite, IOP Conf. Ser. Mater. Sci. Eng. (2017), https://doi.org/10.1088/1757-899X/225/1/012154.

[66] J.J. Elsner, A. Kraitzer, O. Grinberg, M. Zilberman, Highly porous drug-eluting structures: from wound dressings to stents and scaffolds for tissue regeneration, Biomatter (2012) 239–270, https://doi.org/10.4161/biom.22838.

[67] J. Prasad Reddy, J.W. Rhim, Isolation and characterization of cellulose nanocrystals from garlic skin, Mater. Lett. (2014) 20–23, https://doi.org/10.1016/j.matlet.2014.05.019.

[68] S.S. Munawar, K. Umemura, S. Kawai, Characterization of the morphological, physical, and mechanical properties of seven nonwood plant fiber bundles, J. Wood Sci. (2007) 108–113, https://doi.org/10.1007/s10086-006-0836-x.

[69] W. Wang, et al., Electrospun egg white protein/polyvinyl alcohol/graphene oxide fibrous wound dressing: fabrication, antibacterial, cytocompatibility and wound healing assay, Colloids Surfaces A Physicochem. Eng. Asp. (2023), https://doi.org/10.1016/j.colsurfa.2022.130658.

[70] W.C. Lin, C.C. Lien, H.J. Yeh, C.M. Yu, S.H. Hsu, Bacterial cellulose and bacterial cellulose-chitosan membranes for wound dressing applications, Carbohydr. Polym. (2013) 603–611, https://doi.org/10.1016/j.carbpol.2013.01.076.

[71] Y. Luo, et al., Mechanically strong and on-demand dissolube chitosan hydrogels for wound dressing applications, Carbohydr. Polym. (2022), https://doi.org/10.1016/j.carbpol.2022.119774.

[72] H. Chen, et al., A novel wound dressing based on a Konjac glucomannan/silver nanoparticle composite sponge effectively kills bacteria and accelerates wound healing, Carbohydr. Polym. (2018) 70–80, https://doi.org/10.1016/j.carbpol.2017.11.029.

[73] H.A. Begum, T.R. Tanni, M.A. Shahid, Analysis of water absorption of different natural fibers, J. Text. Sci. Technol. (2021) 152–160, https://doi.org/10.4236/jtst.2021.74013.

[74] Y. Wu, et al., Green and biodegradable composite films with novel antimicrobial performance based on cellulose, Food Chem. (2016) 250–256, https://doi.org/10.1016/j.foodchem.2015.10.127.

[75] Y. Han, M. Yu, L. Wang, Physical and antimicrobial properties of sodium alginate/carboxymethyl cellulose films incorporated with cinnamon essential oil, Food Packag. Shelf Life (2018), https://doi.org/10.1016/j.fpsl.2017.11.001.

[76] G.E. Jeyakumar, R. Lawrence, Mechanisms of bactericidal action of Eugenol against Escherichia coli, J. Herb. Med. (2021), https://doi.org/10.1016/j.hermed.2020.100406.